Oscillations in the central brain of *Drosophila* are phase locked to attended visual features

Martyna J. Grabowska[a], Rhiannon Jeans[a], James Steeves[a], and Bruno van Swinderen[a,1]

[a]Queensland Brain Institute, The University of Queensland, Brisbane, QLD 4072, Australia

Edited by Craig Montell, University of California, Santa Barbara, CA, and accepted by Editorial Board Member Michael S. Gazzaniga October 9, 2020 (received for review May 27, 2020)

Object-based attention describes the brain's capacity to prioritize one set of stimuli while ignoring others. Human research suggests that the binding of diverse stimuli into one attended percept requires phase-locked oscillatory activity in the brain. Even insects display oscillatory brain activity during visual attention tasks, but it is unclear if neural oscillations in insects are selectively correlated to different features of attended objects. We addressed this question by recording local field potentials in the *Drosophila* central complex, a brain structure involved in visual navigation and decision making. We found that attention selectively increased the neural gain of visual features associated with attended objects and that attention could be redirected to unattended objects by activation of a reward circuit. Attention was associated with increased beta (20- to 30-Hz) oscillations that selectively locked onto temporal features of the attended visual objects. Our results suggest a conserved function for the beta frequency range in regulating selective attention to salient visual features.

attention | closed-loop behavior | *Drosophila melanogaster* | neuropeptide F | optogenetics

Selective attention refers to the brain's capacity to focus on a subset of stimuli while ignoring others (1). While subjectively intuitive in humans (2), selective attention has also been documented in a wide variety of animals, such as other primates (3), birds (4), and even insects (5). What is attended to depends on stimulus salience (e.g., loudness or brightness), as well as on the perceived value of a stimulus and the motivational state of the animal (1, 6). What is attended to also depends on what is perceived as a singular object. Object-based attention (7, 8) refers to the capacity to direct attention to a conjunction of different features linked as part of the same object. Attending to one feature of a given object would thus enhance not only the neural representation of that particular feature, but also other features that are associated with the object (9). How this form of generalization works is not entirely understood (10) but seems to require some form of feature binding (11) to first determine which stimuli belong together as a unified object (6, 12, 13) and then to link the object to some inherent value, or valence (14). Hence, feature binding appears to be essential for object-based attention (15–17), as neural gain has to be allocated to specific features first in order to perceive an object as a whole. At the same time, distinct stimulus features can become unbound from an attended object if they are selectively ignored (18).

In the mammalian brain, feature binding and object-based attention have been proposed to be associated mechanisms (19), both of which seem to be facilitated by synchronized activity of neuronal assemblies, which can be detected as phase-locked neural oscillations (16, 20–23). In particular, oscillations in the range of 13 to 30 Hz (beta) and 30 to 80 Hz (gamma) seem to reflect this form of binding based on their strong synchronization at various time points following visual or auditory stimulation, with distinct oscillatory processes potentially reflecting different levels of perception. For example, early (<100-ms) stimulus-evoked synchronization in the gamma range has been suggested to represent rapid integration of unconscious sensory processes, whereas later (200- to 400-ms) synchronization in both the beta and gamma range is hypothesized to reflect feature binding and conscious perception (20, 22, 24, 25). Stimulus-evoked beta and gamma oscillations would thus represent a phase reset of ongoing neuronal activity associated with enhancing attentional gain for specific features, by facilitating information transfer or binding among different brain regions (26).

While there is neural evidence for object-based attention in nonhuman primates (27), it is unknown if the smallest animal brains, such as those of insects, combine diverse sensory stimuli into unified percepts, or if they even have a subjective awareness (28). Behavioral studies in honeybees suggest that some insects can detect illusory contours as single objects (29) and can group distinct stimuli into abstract concepts such as "sameness" or "difference" (30), which could indicate a form of categorization through object-based attention. Similarly, visual learning paradigms for *Drosophila melanogaster* have uncovered a capacity for context generalization, where flies perceived visual objects as the same despite changes in color (31, 32), suggesting they were attending to the object shape feature and ignoring color cues. There is growing evidence for attention-like processes in insects, such as during visual fixation, decision making, and novelty detection in *Drosophila* flies (33–36), as well as multiple object tracking in dragonflies (37). The latter electrophysiological study uncovered motion-detecting neurons in dragonflies that selectively lock onto the timing or phase of salient objects, which was shown by "tagging" competing objects with distinct flicker

Significance

There is increasing evidence that even the smallest animal brains provide a capacity for selective attention and subjective awareness, but it is unknown if similar mechanisms might be employed as in higher animals. Recent work in insects highlights a brain structure, the central complex (CX), which could support selective attention processes. Recording from the CX of behaving flies making decisions in a virtual reality environment, we show that visual selection is achieved by phase-controlled endogenous 20- to 30-Hz oscillations that lock onto temporal features of attended visual objects. This suggests an oscillation-driven binding mechanism in the insect brain that employs a similar beta frequency range as has been observed for feature binding in humans.

Author contributions: M.J.G., R.J., and B.v.S. designed research; M.J.G., R.J., and J.S. performed research; M.J.G. contributed new reagents/analytic tools; M.J.G. and R.J. analyzed data; and M.J.G. and B.v.S. wrote the paper.

The authors declare no competing interest.

This article is a PNAS Direct Submission. C.M. is a guest editor invited by the Editorial Board.

[1]To whom correspondence may be addressed. Email: b.vanswinderen@uq.edu.au.

This article contains supporting information online at https://www.pnas.org/lookup/suppl/doi:10.1073/pnas.2010749117/-/DCSupplemental.

First published November 11, 2020.

frequencies (37). However, it is unknown how such selective neural processes are controlled in the insect brain or whether these neural measures are relevant to behavioral decision making.

It is possible that the insect brain, like the mammalian brain, employs oscillatory activity and stimulus-evoked phase locking to prioritize and bind stimulus features, and to enhance attentional gain. Indeed, earlier electrophysiological studies revealed oscillatory activity in the 20- to 30-Hz range in the *Drosophila* brain that was associated with detecting salience effects, such as visual novelty (38–40), suggesting that these endogenously generated oscillations might be more broadly involved in regulating attention-like processes in the fly brain (41). However, it remained unclear which neurons might be generating these oscillations. One likely neuropil is the central complex (CX), a heterogeneous structure in the central brain that has been associated with visual pattern learning (42–44). Recent studies in behaving *Drosophila* also identified the CX as a key brain region for visual navigation (45, 46). This suggests a broader role for the CX in directing attention-like processes (5), which could also reflect ring attractor dynamics within CX circuits (47, 48). While its role in visual perception is increasingly evident, whether the CX produces neural oscillations relevant to visual attention and feature binding is unknown. To address this question requires not only measuring electrical activity in the CX of behaving flies, but also correlating any endogenous brain activity to distinct neural signatures associated with competing visual stimuli or stimulus features.

In tethered virtual reality experiments, flies tend to fixate on large objects and avoid small objects, whether they are flying (49) or walking (33). We exploited this innate visual dichotomy to examine mechanisms underlying visual selective attention in *Drosophila*. To disambiguate between the attractive and aversive stimuli in the fly brain, and to relate neural activity to ongoing behavioral choices, we recorded local field potentials (LFPs) from the CX and made the competing visual stimuli flicker at distinct frequencies, thereby evoking steady-state visually evoked potentials (SSVEPs) in the fly brain. We first showed that the SSVEPs varied in amplitude depending on the visual objects being fixated upon, allowing us to then investigate how attention guided the binding of different visual features, such as object size, brightness, and flicker frequency. By calculating phase-locking strength between the distinct SSVEPs and endogenous brain activity, we then examined how oscillations in the CX interacted with one another. We found frequency-specific phase locking between endogenous oscillations in the 20- to 30-Hz frequency range and the object features that the fly paid attention to, suggesting that beta-like oscillations could be employed for object-based attention in the insect brain.

Results

***Drosophila* Flies Generalize Visual Object Preferences.** To investigate visual attention in *Drosophila*, we exploited the flies' innate attraction to large objects and aversion to small objects (33, 49). This innate preference (or valence) differential based on object size provided a well-grounded starting point to probe visual responsiveness in our brain recording paradigm. To demonstrate visual responsiveness behaviorally, tethered female flies controlled the angular position of a virtual object in a wraparound arena of light-emitting diodes (LEDs) (Fig. 1*A*) by walking on an air-supported ball under closed-loop feedback conditions (33, 50–52). The 360° visual scene consisted of two objects locked 180° apart, an attractive large green bar (height: 60°, width: 15°, luminosity: 110 or 579 lx) and an aversive small green bar (height: 26.5°, width: 15°, luminosity: 67 or 301 lx) on an unlit background (Fig. 1*B*). Under closed-loop conditions, we define an object as attractive when flies maneuver the ball to place the object in their frontal visual field (FVF), a behavior known as fixation (33). We define an object as aversive when it is placed behind by the fly. Randomly timed perturbations of the visual scene (60° to the left or to the right) (Fig. 1*C*) ensured that the flies actively attended to the virtual objects and thus recurrently displayed their fixation preference (33, 50). To track brain activity in this context, we recorded LFPs from the CX, a neuropil in the central brain that has been associated with visual processing (42–44, 53) (Fig. 1*D*, *Materials and Methods*, and *SI Appendix*, Fig. S1). Having previously shown that flies preferred to place the large bar in front and the small bar behind them [even when presented on their own (33)], we added additional visual features to these objects by changing their brightness (contrast) and making them flicker at distinct frequencies (5.9 or 6.6 Hz) (*Materials and Methods* has brightness and flicker characteristics). We presented all combinations of these three visual features (size, brightness, and flicker frequency) in competition, in a counterbalanced design (Fig. 1*B* and *Materials and Methods*). This allowed us to determine if object size preferences persisted despite the layering of additional features or if these added visual features altered the innate preference assigned to these objects. We found that flies still fixated preferentially on the large bar, irrespective of brightness or flicker frequency (Fig. 1 *E* and *F* and *SI Appendix*, Fig. S2). This suggests that the valence cue provided by the size of the object dominates over the other visual features or alternatively, that these other features become associated with the valence innately linked to object size. Together with our previous work showing that flies also fixate preferentially on large dark (unlit) bars in a bright background (33), this confirms that object size or shape is driving fixation choices in this paradigm. When object size is kept constant, flies prefer high-contrast objects in this paradigm (33). Here, a brighter, high-contrast small bar was still less attractive than a darker, low-contrast large bar (Fig. 1*F* and *SI Appendix*, Fig. S2).

Neural Gain Is Linked to the Valence of an Attended Visual Object. We next determined how the flies' LFP activity in the CX covaried with their fixation behavior (Fig. 1*C*). We examined LFP power at the two distinct flicker frequencies (5.9 and 6.6 Hz), counterbalanced for all conditions. Visual flicker produces SSVEPs (or "frequency tags") in the brains of insects as well as humans, and the amplitude of SSVEPs has been shown to be modulated by attention (36, 37, 54). The flicker frequencies we employed in this study were selected because they produce robust SSVEPs in the fly central brain (Fig. 1*C* and *SI Appendix*, Fig. S3*A*) and are in a range that evoked no innate behavioral preferences compared with other frequencies (*Materials and Methods* has a description of how frequency preferences were determined; *SI Appendix*, Fig. S3*B*). We found that the larger (attractive) bar evoked greater LFP power on average than the smaller (aversive) bar when either of these was in the FVF, irrespective of the brightness of the stimulus (high vs. low) (Fig. 1*G*, data pooled for both flicker frequencies; *SI Appendix*, Fig. S4*A* shows separated frequency data). As with the behavioral experiments, this suggests that object size determines the LFP response and that added visual features such as brightness or flicker are subsumed by this primary visual feature. When we compared LFP responses to identical objects of different brightness (e.g., two large bars, pooled for both flicker frequencies), we found no significant difference in power when either object was fixated upon in the FVF (Fig. 1*H* and *SI Appendix*, Fig. S4*B*). However, when we examined the LFP responses when the same objects were not being fixated upon (in the periphery, outside the FVF), we observed increased LFP power for the brighter and potentially more salient objects (Fig. 1*I* and *SI Appendix*, Fig. S4*B*) and no difference for the distinct frequencies (*SI Appendix*, Fig. S4*A*). These electrophysiological findings support our behavioral data, showing that object cues dominate over brightness cues when flies are actively fixating by placing preferred objects in their FVF. Importantly, the fixated object determines which flicker frequency evokes a

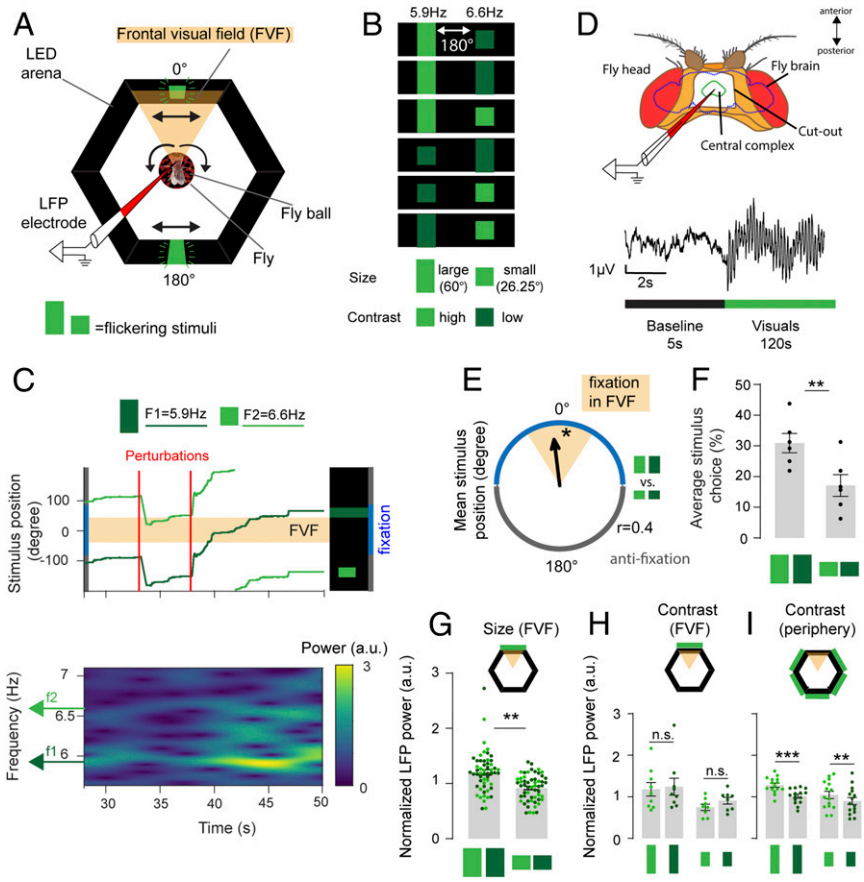

Fig. 1. Neural gain is bound to the valence of an attended visual object. (*A*) Experimental setup for closed-loop paradigm. Arrows indicate image movement linked to ball rotated by the fly. LFP, local field potential. (*B*) Competing visual object pairs vary in size, flicker frequency, and contrast. Twelve pairwise combinations were tested (*Materials and Methods*). (*C*) Example for fixation behavior during 60° perturbations in one fly. (*C*, *Upper*) Stimulus positions over time (light green = small high-contrast 6.6-Hz bar; dark green = large low-contrast 5.9-Hz bar). (*C*, *Lower*) Spectrogram for the same fly showing LFP power over time for both flicker frequencies f1 and f2. Stimuli are locked to be 180° apart. (*D*, *Upper*) LFPs were recorded from the CX of the fly brain through a window in the cuticle of the fly head. (*D*, *Lower*) Experiments consisted of 5-s baseline and 120-s visual stimulation. (*E*) Mean stimulus position for all experiments where the large and small bars were tested together, 180° apart (Rayleigh test for directionality, $*P < 0.05$; $n = 6$). Polar plot shows mean vector length, with 0° indicating the large bar is in front of the fly. (*F*) Average stimulus choice for large vs. small bars, pooled for both contrasts and frequencies (Wilcoxon rank sum test, $n = 6$, error bars = SEM). (*G*) Mean normalized LFP power of large and small visual objects placed in the FVF by the animals (data points show individual trials for high-contrast [bright green] and low contrast [dark green] visual stimuli; Wilcoxon rank sum test on averaged data for $n = 6$ animals, error bars = SEM). (*H*) Normalized LFP power for large and small bars, extracted from instances where stimulus was in the FVF for high- and low-contrast stimuli (data points show individual trials for high-contrast [bright green] and low-contrast [dark green] visual stimuli; Wilcoxon rank sum test between contrasts on averaged data for $n = 6$ animals). (*I*) Normalized LFP power for large and small bars, extracted from instances where the stimulus was at any position in the arena except the FVF, for high- and low-contrast stimuli (data points show individual trials for high-contrast [bright green] and low-contrast [dark green] visual stimuli; Wilcoxon rank sum test between contrasts on averaged data for $n = 6$ animals). All animals were dNPF-Gal4; UAS-CSChrimson(x)::mVenus flies that have not been fed all trans-Retinal (ATR−). $n = 6$. n.s., not significant. $**P < 0.01$; $***P < 0.001$.

greater SSVEP in the fly brain (Fig. 1*G*). These results suggest that neural gain in the CX is linked to the valence of an attended visual object.

Increased Neural Gain for the Preferred Object Persists under Passive Viewing Conditions. The above results demonstrate that an innately attractive object (a large bar) evokes a greater LFP response in the fly central brain than an aversive object (a small bar). However, these experiments were done under closed-loop conditions, where the fly was in control of the object on which it decides to fixate (flies also fixate on the aversive object some of the time) (Fig. 1*C*). We therefore next asked if the differential neural responses assigned to the attractive and aversive bar persisted under "open-loop" conditions, when the fly was not in control. To test this, we placed both objects (large and small) side by side in the FVF for the flies to observe passively while we recorded their brain activity (Fig. 2*A*). As before, we tagged both objects with distinct flicker frequencies (5.9 or 6.6 Hz) and counterbalanced these for brightness (*Materials and Methods*) and position (left vs. right) (Fig. 2*B*). As both objects remained in the FVF, these evoked continuously robust SSVEPs in the central brain (Fig. 2*C*: in this example, f2 = frequency tag associated with the large bar). Under these passive viewing conditions, we found that the attractive object (the large bar) still evoked a stronger neural response than the aversive object (the small bar), irrespective of left or right position (Fig. 2*D*), flicker frequency (Fig. 2*E*), or stimulus brightness (Fig. 2*F*).This shows that the valence differential based on object size that we observed in closed loop persists in open loop (Fig. 2*G*). One interpretation of these results is that flies in this open-loop context are attending more to the larger attractive bar, which is reflected in its greater frequency tag, even if they cannot control the bar's position in the arena.

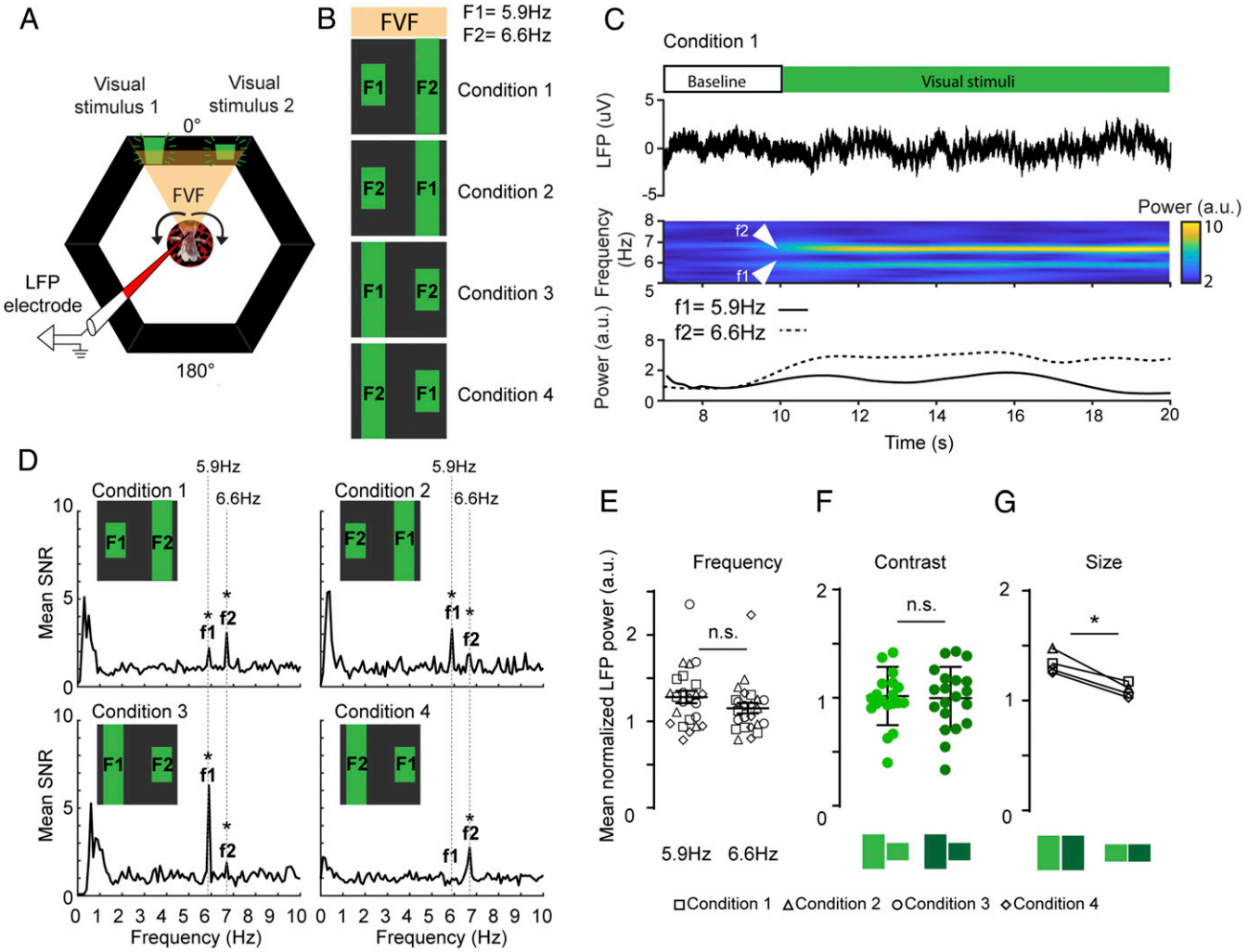

Fig. 2. A preferred visual object evokes greater neural gain during passive viewing. (*A*) Open-loop paradigm. Both visual stimuli are presented to the fly in the FVF, while the LFP is recorded from the CX (Fig. 1). Arrows indicate the fly moving the ball, while visual stimuli stay fixed in the FVF. (*B*) Flies are presented with four flicker/position/object conditions. These conditions vary in contrast (*Materials and Methods*). F1 and F2 are flicker frequencies. (*C*, *Upper*) Each trial consists of a 10-s baseline and a 20-s stimulation period. (*C*, *Lower*) Example for one trial (n = 1) showing the LFP trace (top trace), the time–frequency spectrogram with increased power for both input frequencies (middle trace), and the averaged power for both input frequencies (bottom trace). (*D*) Signal-to-noise ratio (SNR) of power spectra averaged across all trials for all animals (f1, f2 = output frequencies of F1, F2, respectively). (*E*) Normalized LFP power for visual stimuli with the same input frequencies F1 = 5.9 and F2 = 6.6 for all conditions (Wilcoxon rank sum test, error bars = SEM). (*F*) Normalized LFP power for high- and low-contrast stimuli (Wilcoxon rank sum test, error bars = SD). (*G*) Normalized LFP power for large (high/low contrast) and small (high/low contrast) for all four conditions (Wilcoxon matched pair rank test). n = 6. All animals are dNPF-Gal4; UAS-CSChrimson(x)::mVenus flies that have not been fed all trans-Retinal (ATR−). n.s., not significant. *P < 0.05.

Optogenetic Activation of a Reward Circuit Modulates Visual Attention in Closed-Loop Experiments. A question that arises from the preceding results is whether the neural response to the large bar is greater simply because it is a larger object, which may also explain why larger bars evoke more fixation behavior than smaller bars. To disambiguate innate preferences from simple size effects would require identifying a small object that flies find attractive or a large object that they find aversive. Alternatively, the attractiveness of either bar could be altered by changing the motivational state of the flies when they fixated on either stimulus. We decided on an optogenetic strategy to increase the attractiveness of the small bar by activating a putative reward circuit in the fly brain (33, 55, 56) whenever the small bar was fixated upon. In a previous behavioral study in *Drosophila*, we have shown that an aversive object (a small bar) could be rendered more attractive by optogenetic activation of neurons that express *Drosophila* neuropeptide F (dNPF) in the fly brain (33). dNPF is the homolog of mammalian neuropeptide Y (57), which is involved in the regulation of emotional responses (58). In flies, dNPF function has been associated with aggression (59), reward (55), and arousal (60). dNPF-expressing neurons provide neuromodulatory input to various regions of the fly brain, including the CX (56), which has been proposed to influence value-based decision making (55). A notable target of dNPF modulation in the CX is the fan-shaped body (FB) (55, 56), which was made clearly visible with mVenus expression in dNPF neurons and was used as a signal to guide the positioning of our recording electrode (Fig. 3*A*, *Materials and Methods*, and *SI Appendix*, Fig. S1). We hypothesized that rendering the small bar more attractive via dNPF circuit activation should increase neural responsiveness to it, which would manifest in the amplitude of SSVEPs. To activate the dNPF circuit, we expressed a red-shifted channel rhodopsin (CsChrimson) (61) in flies that had been fed 0.2 mM all trans-Retinal (ATR+) (*Materials and Methods*). Acute activation was achieved with red light emitting diodes (LEDs), which illuminated the tethered fly in

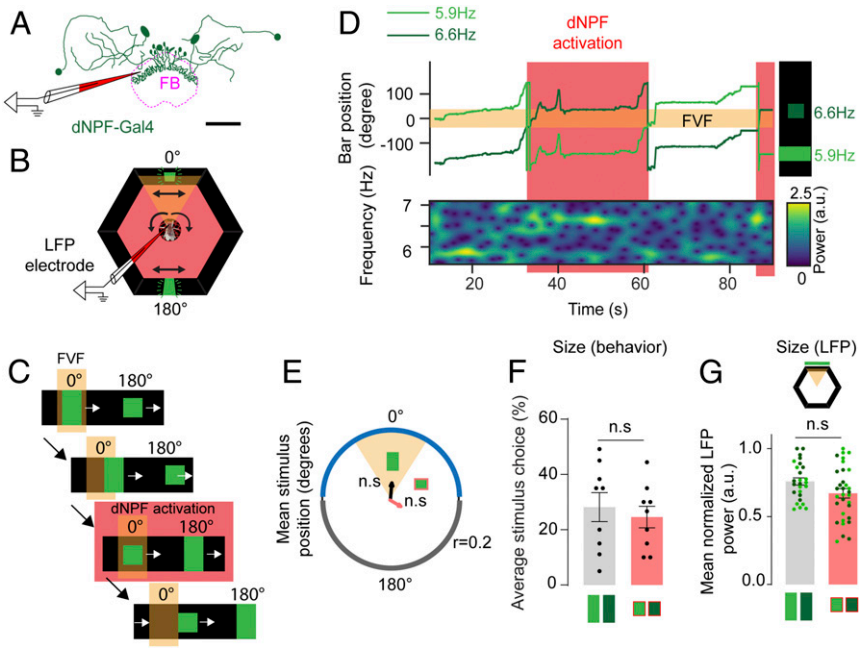

Fig. 3. Optogenetic activation of a dNPF circuit abolishes aversion to the small bar. (*A*) dNPF-Gal4 circuit. dNPF neurons project to the fan-shaped body (FB). LFPs are recorded from the vicinity of the FB. (Scale bar: 50 μm.) (*B*) Closed-loop setup. dNPF circuit activation is achieved with red LEDs surrounding the arena. Black arrows indicate fly ball and bar movements. (*C*) Experimental paradigm. Triggering of red LEDs is achieved when the small bar enters the FVF. Red LEDs stay on as long as the small bar is in the FVF. (*D*) Example for one fly. Fixation on the small bar in the FVF triggers dNPF circuit activation. A small bar in the FVF is associated with an increase in LFP power for the corresponding input frequency, 6.6 Hz. (*E*) Mean stimulus position of the large and small visual stimuli for pooled trials of all animals (Rayleigh test for directionality, $n = 9$, ATR+); 0.2 = axis for mean vector length *r*. (*F*) Average stimulus choice for large vs. small bar, pooled for both contrasts and frequencies (Wilcoxon rank sum test, $n = 9$, ATR+, error bars = SEM). (*G*) Normalized LFP power for each bar size (Wilcoxon rank sum test on averaged LFP power for corresponding stimulus positions of each animal, $n = 9$, ATR+, error bars = SEM, data points represent individual instances of averaged LFP power for the corresponding stimulus within the highlighted positions in the LED arena). Red color indicates red LED activation. All animals are dNPF-Gal4; UAS-CSChrimson(x)::mVenus that have been fed all trans-Retinal (ATR+). n.s., not significant.

the arena (Fig. 3*B*). To test that the optogenetic manipulation was working, we performed closed-loop fixation experiments in our brain recording preparation, where we acutely activated dNPF circuits whenever the fly fixated on the small bar (Fig. 3 *C* and *D* and *Materials and Methods*). We confirmed that dNPF activation eliminated innate aversion to the small bar (Fig. 3 *E* and *F*), as shown previously (33). Interestingly, this induced change in behavior also eliminated any significant differences in neural responses between the fixated objects under closed-loop conditions (Fig. 3*G*), showing that object size alone did not determine SSVEP amplitudes.

Activation of the dNPF Circuit Redirects Salience to an Aversive Object in Open-Loop Experiments. We next investigated how dNPF circuit activation affects brain responses when flies are not able to control the position of the visual objects. We recorded LFPs in flies that were presented with both objects fixed in their FVF (in open loop), counterbalanced for flicker frequency, contrast, and position (Fig. 4*A*), as before (Fig. 2*B*). Following our closed-loop results above, we expected the frequency tags associated with either object to be similar in amplitude when the dNPF circuit was activated. However, we found that in the open-loop context, the smaller bar evoked a stronger neural response than the larger bar, irrespective of the frequency tag employed, the brightness, or the object position (Fig. 4*B*). This is the opposite of what we saw in the control (ATR−) condition (Fig. 4*C*) and shows that dNPF circuit activation can completely overturn innate salience assignations. More generally, these results confirm that larger objects do not necessarily evoke greater responses in the fly brain. Rather, as in the human brain (62), attention probably regulates SSVEP responses in the fly central brain, with neuromodulatory circuits playing an important role in determining associated neural gain.

The preceding results could suggest that dNPF activation causes flies to redirect their attention from the large bar to the small bar when they cannot control the angular position of the objects. We wondered if this potential switch in attention could nevertheless be verified by tracking walking behavior. To address this, we conducted open-loop behavioral experiments to determine if dNPF activation increased turning bias in the direction of the more salient small bar (Fig. 4*D* and *SI Appendix*, Fig. S5). Since the two competing objects were in the FVF and therefore, unlikely to evoke a strong left–right bias, we also tested a second open-loop configuration where the competing objects were farther apart, and we counterbalanced for all object size, brightness, and flicker frequency combinations (*SI Appendix*, Fig. S5*A*). Determining a fictive track per fly allowed us to assess their left/right walking preferences for each condition (Fig. 4*D*). As found previously (33), dNPF activation makes flies walk more slowly (*SI Appendix*, Fig. S5*B*). However, dNPF activation during open loop did not bias flies to turn toward either bar, on average (Fig. 4*E* and *SI Appendix*, Fig. S5*C*). Instead, flies increased their walking speed specifically when they were confronted with competing small and large bars (Fig. 4*F*), a behavior that was not observed in control animals (*SI Appendix*, Fig. S5*D*). This suggests that the increased SSVEP assigned to the small bar during dNPF activation in open loop is associated with increased walking speed rather than altered turning behavior.

Activation of the dNPF Circuit Promotes Selective Endogenous Oscillations. We observed that dNPF activation appeared to increase overall LFP power in the fly brain, in addition to redirecting salience to the competing smaller object (Fig. 4*C*). We confirmed this by examining SSVEP power for each object separately, compared with nonactivated controls (*SI Appendix*,

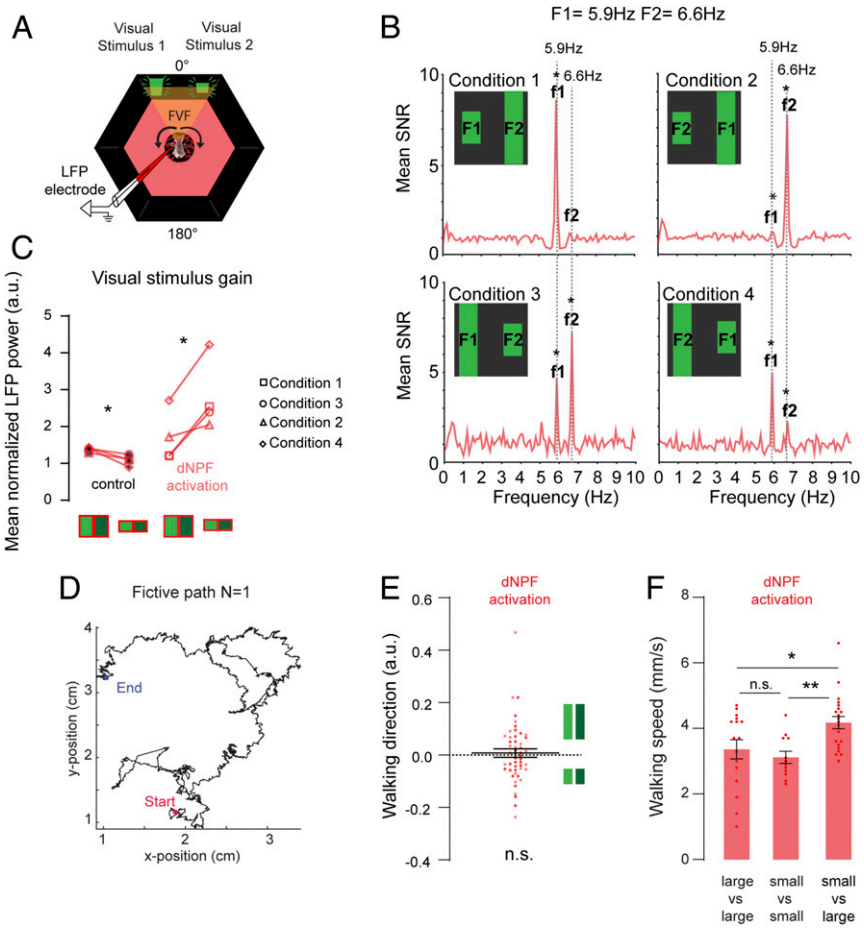

Fig. 4. (*A*) Optogenetic activation of dNPF neurons was achieved by illuminating the fly in the arena with red LEDs (*Materials and Methods*). (*B*) Signal-to-noise ratio (SNR) of power spectra averaged across all trials for all animals (f1, f2 = output frequencies of F1, F2, respectively; $n = 7$, ATR+). (*C*) Normalized LFP power per condition for large and small bars (high and low contrast) for controls (ATR−; red light, red/black) and optogenetic dNPF activation (ATR+; red light, red; Wilcoxon matched pair rank test, $n = 7$). (*D*) Example fictive path of a 2-min trial for one fly in open-loop conditions, calculated from the rotations of the ball by the walking fly. (*E*) Mean fly walking direction, pooled for dark and bright large (*Upper*) and small (*Lower*) bars. (*F*) Mean walking speed for all conditions, averaged across flies pooled for large vs. large, small vs. small, and small vs. large bar conditions for both open-loop configurations [one-way ANOVA F(DFn,dFd) = 6.064 (2, 46), $P = 0.0046$, Tukey's multiple comparisons test]. All animals are dNPF-Gal4; UAS-CSChrimson(x)::mVenus flies. n.s., not significant. $*P < 0.05$; $**P < 0.01$.

Fig. S6). The overall increase in LFP activity suggested a broadly deployed gain-control mechanism regulated by the dNPF circuit. To further investigate this potential mechanism, we examined the effect of dNPF circuit activation under baseline conditions, when no visual stimuli were present. Under baseline conditions, dNPF circuit activation resulted in an overall increase in LFP power (0.2 to 100 Hz) in the CX (Fig. 5*A*). This suggested a broad effect on neural gain across a wide range of endogenous LFP frequencies; an increase in overall endogenous LFP activity may explain why SSVEP power is increased for both frequency tags simultaneously. It does not explain, however, why SSVEPs are increased proportionally more for the smaller bar, under dNPF circuit activation.

Given that dNPF circuit activation powerfully modulated visual responsiveness, we pursued this controlled optogenetic approach to arrive at a better understanding of how object-based attention operates in the fly brain and what role endogenous oscillations might have in selecting one stimulus vs. another. In humans, endogenous oscillations have been proposed to act as a perceptual binding mechanism in the brain for a variety of frequency ranges such as alpha (7 to 14 Hz) (63), beta (15 to 30 Hz) (64), and gamma (30 to 80 Hz) (65). We, therefore, examined more closely the effect of dNPF circuit activation on endogenous oscillations in the fly brain, under the open-loop conditions that produced such strong selective responsiveness to the small bar (Fig. 4 *B* and *C*). We partitioned baseline endogenous brain activity recorded from the CX into five frequency ranges (10 to 20, 20 to 30, 30 to 40, 40 to 50, and 50 to 100 Hz) and found a significant increase for all frequencies between 10 and 50 Hz during dNPF activation (Fig. 5 *B*–*E*) but not 50 to 100 Hz (Fig. 5*F*). We then asked whether adding visual stimuli (during dNPF activation) evoked any additional LFP effects within these endogenous frequencies and found a further increase specifically in the beta range (20 to 30 Hz) (Fig. 5*C*). As endogenous beta-like oscillations have previously been associated with visual salience in *Drosophila* (39, 40), this suggested that the dNPF circuit might be regulating visual attention by controlling 20- to 30-Hz activity in the CX.

To investigate the interplay between endogenous and evoked LFP activity in the CX, we performed phase–amplitude correlation analyses between all endogenous frequency amplitudes (0.2 to 100 Hz) and the phases of the competing frequency tags (5.9 and 6.6 Hz) to measure the envelope to signal correlation (ESC) (66–68) (*Materials and Methods* and *SI Appendix*, Fig. S7). A positive correlation in this analysis indicates a modulatory link between the endogenous and evoked oscillations. We found a

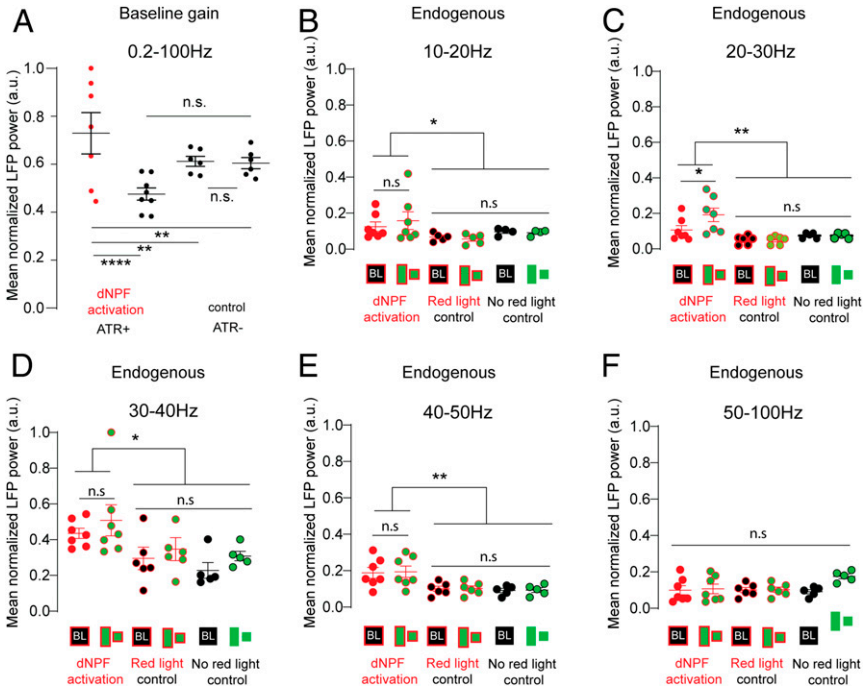

Fig. 5. (*A*) Mean normalized baseline gain (no visual stimulation, 0.2 to 100 Hz) for control (ATR−; red light [black], $n = 6$) and during dNPF circuit activation (ATR+; red light [red], $n = 7$; Wilcoxon rank sum test, error bars = 95% CIs of the mean). (*B–F*) Mean normalized LFP power (normalized to maximum value) of filtered endogenous frequency bands compared between two controls (ATR−, no red light, $n = 5$ and ATR−, red light, $n = 6$) and dNPF circuit activation (ATR+, red light, $n = 7$). Data show means across all trials per fly, ± SEM. ANOVAs: 10 to 20 Hz: $P = 0.048$, F(DFn,DFd) = 1.89 (7, 42); 20 to 30 Hz: $P = 0.003$, F(DFn,DFd) = 1.751 (7, 42); 30 to 40 Hz: $P = 0.0106$, F(DFn,DFd) = 0.4802 (7, 42); 40 to 50 Hz: $P = 0.0056$, F(DFn,DFd) = 1.086 (7, 42); 50 to 100 Hz: not significant (n.s.) $P = 0.99$, F(DFn,DFd) = 0.878 (7, 42). Tukey's multiple comparison test. All animals are dNPF-Gal4; UAS-CSChrimson(x)::mVenus flies that were either fed all trans-Retinal (ATR+) or not (ATR−). BL, baseline. $*P < 0.05$; $**P < 0.01$; $****P < 0.0001$.

significant correlation between endogenous LFP activity (at ∼30 Hz) and the phase of the visually evoked oscillations during visual stimulation (Fig. 6*A* and *SI Appendix*, Fig. S8). This suggested that the increased endogenous 20- to 30-Hz activity seen during visual stimulation (Fig. 5*C*) might be involved in selecting which visually evoked tag was bound to the attended percept. Knowing that dNPF circuit activation dramatically increased neural responsiveness to the small bar in this experiment (Fig. 4 *B* and *C*), we then examined if 20- to 30-Hz oscillations were specifically associated with this effect. Indeed, we found that optogenetic activation of the dNPF circuit during visual stimulus presentation specifically increased the mean ESC between endogenous 20- to 30-Hz activity and the visually evoked tags (Fig. 6*B*). Significant ESC effects for higher gamma-like frequencies (30 to 50 Hz) were also observed when the visual stimuli were present (Fig. 6*B*), but only 20 to 30 Hz showed an increased correlation to the evoked frequency tags upon dNPF circuit activation. This suggests a specific role for endogenous beta-like (20- to 30-Hz) oscillations in valence-driven stimulus selection.

How might endogenous beta-like activity be selecting one evoked tag over another, when these are associated with a more salient object? Although our ESC calculations highlighted endogenous 20- to 30-Hz activity as a potential driver of the frequency tags during dNPF circuit activation, this did not discriminate between the two different tags. Given that dNPF circuit activation increased neural responses to the smaller bar (Fig. 4 *B* and *C*) and that this was associated with increased 20- to 30-Hz activity (Fig. 6*B*), we hypothesized that frequency tags associated with the smaller bar should be more correlated to endogenous 20- to 30-Hz activity. To investigate this, we performed phase-locking analyses between endogenous 20- to 30-Hz activity and the evoked frequency tags assigned to either object to determine a phase-locking value (PLV) (*Materials and Methods* and *SI Appendix*, Fig. S7). We found that dNPF activation specifically increased the PLV between endogenous 20- to 30-Hz activity and the tag associated with the smaller bar, compared with the larger bar (Fig. 6*C*), irrespective of the stimulus frequency. This suggests that under passive viewing conditions, increased neural responsiveness to the small bar is associated with endogenous beta-like activity phase locking specifically to the visual flicker associated with the small bar. dNPF circuit activation appears to drive this effect, as increased phase locking was not observed under control conditions in open loop (Fig. 6*C*).

Endogenous 20- to 30-Hz Oscillations Lock onto the Visual Features of an Attended Object. Our results suggest that 20- to 30-Hz oscillations in the CX of *Drosophila* might be employed to drive visual salience effects by increasing the SSVEP gain for the small bar. To determine if this was indeed an attentional mechanism modulated by endogenous beta-like activity, we examined dNPF activation effects under closed-loop conditions, when the fly could demonstrate its visual choices behaviorally. Specifically, we examined brain activity during fixation events when flies returned the smaller bar to the FVF after a perturbation (Figs. 1*C* and 6*D*), which was promoted by dNPF circuit activation (Fig. 3). Consistent with an attentional effect, we detected increased 20- to 30-Hz activity when dNPF-activated flies returned the small bar to the FVF (Fig. 6*E*). Significantly increased 20- to 30-Hz activity was already evident ∼250 ms after a perturbation (Fig. 6*E*; *SI Appendix*, Fig. S9 shows other frequency domains). Transiently increased 20- to 30-Hz activity was associated with increased power in the evoked 5.9- or 6.6-Hz frequency tags when either of these was associated with the small object (Fig. 6*F*). Interestingly, significance for either tag power was only evident ∼1,000 ms after the perturbation (Fig. 6*F*), suggesting

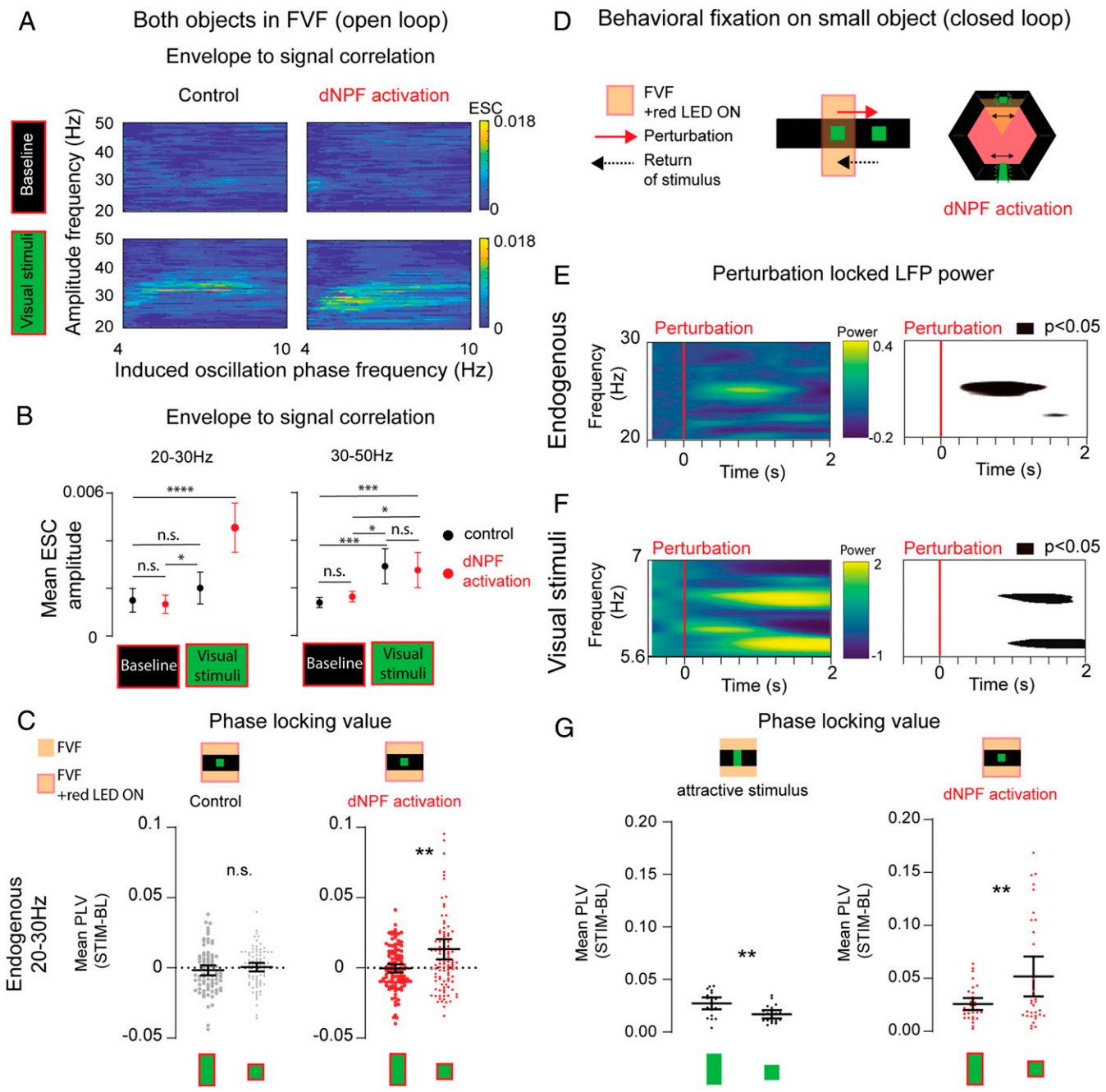

Fig. 6. Endogenous 20- to 30-Hz oscillations are phase locked to selected visual objects. (*A*) Comodulation maps of ESCs during open-loop experiments. The panels show significant positive correlations between endogenous amplitude frequencies (20 to 50 Hz) and the phase of induced frequencies (4 to 10 Hz are shown) for baseline and visual stimulation conditions. Control: ATR−, red LED light, $n = 6$. dNPF activation: ATR+, red LED light, $n = 7$ (Pearson's correlation). (*B*) Mean ESC amplitude between 20 to 30 Hz (*Left*), 30 to 50 Hz (*Right*), and phase of frequency tags (4 to 10 Hz) during baseline and visual stimulation conditions. Control: ATR−, red LED light, black, $n = 6$. dNPF activation: ATR+, red LED light, red, $n = 7$. Repeated measures one-way ANOVA: 20 to 30 Hz: $P < 0.0001$, degrees of freedom = 3, $F(1.863, 190.1) = 15.98$; 30 to 50 Hz: $P < 0.0001$, degrees of freedom = 3, $F(2.413, 251.0) = 11.39$; both: comparisons for differences between individual groups were analyzed using the false discovery method of Benjamini and Hochberg. (*C*) Mean PLVs of evoked frequencies of visual objects with endogenous 20- to 30-Hz activity. Baseline PLV values were subtracted from values during visual stimulation. Control (*Left*): ATR−, red light, black, $n = 6$, trials = 80 ($P = 0.3307$, effect size =0.15). dNPF activation: ATR+, red light, red, $n = 7$, trials = 109 ($P = 0.009$, effect size =0.51; paired t test [two tailed], bootstrapped data showing means with 95% CIs). (*D*) Behavioral fixation on small bar after perturbation in closed loop, causing dNPF activation. (*E*, *Left*) Spectrogram showing mean LFP power over time for endogenous 20- to 30-Hz activity, following a perturbation. (*E*, *Right*) Map showing P values significantly different ($P < 0.05$) from preperturbation baseline (ATR+, red light, $n = 9$, z-scored data). (*F*, *Left*) Spectrogram showing mean LFP power over time for evoked frequencies during visual stimulation. (*F*, *Right*) Map showing P values significantly different ($P < 0.05$) from preperturbation baseline (ATR+, red light, $n = 9$). (*G*) Mean PLV of evoked frequencies of visual objects and endogenous 20 to 30 Hz. Baseline PLV values were subtracted from values during visual stimulation. Control (*Left*): ATR+, no red light; flies return the large visual object to the FVF. $n = 9$, perturbation events = 19 ($P = 0.004$, effect size =1.03), successful perturbations. dNPF activation (*Right*): ATR−, red light, flies return the small visual object to the FVF, $n = 7$, perturbation events = 32 ($P = 0.009$, effect size =0.7667), successful perturbations (paired t test [two tailed], bootstrapped data showing means with 95% CIs, data were tested for skewness: 0.95 and showed a log-normal distribution [Shapiro–Wilk test, $P = 0.06$, $\alpha = 0.05$, resampling data with 1,000 permutations showed no bimodal distribution]). $n = 9$. All animals are dNPF-Gal4; UAS-CSChrimson(x)::mVenus flies that were either fed all trans-Retinal (ATR+) or not (ATR−). BL, baseline; n.s., not significant; Stim, stimulus. *$P < 0.05$; **$P < 0.01$; ***$P < 0.001$; ****$P < 0.0001$.

these followed the 20- to 30-Hz response. We next examined if 20- to 30-Hz activity might be selecting the tag specifically bound to the attended small object. To determine this, we again analyzed phase locking between endogenous 20- to 30-Hz and the evoked frequency tags to calculate a PLV for either visual object. Under control conditions, when dNPF is not activated, flies return the preferred large bar to the FVF following a perturbation (Fig. 1) (33). We found that this behavior was associated with a significant increase in phase locking between endogenous 20- to 30-Hz oscillations and the evoked frequency tags bound specifically to the large bar (Fig. 6*G* and *SI Appendix*, Fig. S10). In contrast, when flies returned the small bar to the FVF (induced by dNPF circuit activation) (Fig. 3), the PLV between 20- to 30-Hz oscillations and the evoked frequency tags bound to the small bar increased significantly (Fig. 6*G*). This effect was not observed in control animals where the optogenetic mechanism was not activated (*SI Appendix*, Fig. S11). These results suggest that endogenous 20- to 30-Hz activity locks onto the precise temporal features (i.e., the flicker frequencies) associated with an attended object and that this capacity for object-based attention is promoted by dNPF circuits in the fly brain.

Discussion

The brain's ability to link complex patterns of sensory input into coherent objects has been termed the binding problem (13), with the "problem" being that it remains unclear how diverse sensory streams are unified into a single conscious percept. Our subjective experience of the world is of discretely bound units rather than segregated sensory streams, and this capacity of the human brain is probably adaptive as sensory cues are often correlated, such as voices with faces (69) or fruits with colors (70). The adaptive advantage of perceiving the world in such a unitary fashion raises the question of whether other brains do this (28) and if so, whether the selective attention mechanisms observed in simpler animals such as insects facilitate a form of feature binding.

In humans, the modulation of endogenous beta (15- to 30-Hz) oscillations is associated with the perception and integration of visual stimuli (71), as well as decision making (72), among other cognitive functions (73). Intriguingly, beta oscillations have also been associated with task-related engagement and reward processing as well as stimulus-locked attentional load effects (20, 74, 75). However, a full understanding of how beta oscillations are deployed to achieve these functions is lacking, and there remains debate regarding their functional role (75). Our finding beta-like oscillations involved in object-based attention in the insect brain lends support to the view that these oscillations perform a conserved function relevant to perception, as it seems unlikely that a completely different neuroanatomy (an insect brain) would have preserved a neural epiphenomenon. Consistent with a causal role for oscillations in the insect brain, we found that dNPF circuit activation in *Drosophila* increased 20- to 30-Hz activity in the CX, which promoted phase locking to attended visual stimuli. Interestingly, in open-loop conditions dNPF activation seemed to produce a valence reversal, suggesting that attention was redirected covertly to the smaller, aversive object. Why the smaller object should have higher value in this specific open-loop context remains unclear. An alternative interpretation of this result is that salience for the smaller object was increased, rather than it having been rendered more attractive. Thus, the dNPF circuit might be more involved with regulating salience rather than valence (76), and the salience of the aversive small bar could thus have been magnified by dNPF activation in open-loop conditions, when the fly is not in control. Interestingly, the increased salience assigned to the competing small bar was associated with increased walking speed, suggesting a motivation to respond behaviorally. Electroencephalography (EEG) studies have found that when humans have no control over an array of emotionally laden visual images, these images evoke a higher SSVEP response compared with emotionally neutral images; however, strongly aversive images evoked the greatest SSVEP responses of all (62). Perhaps similarly in the fly brain, an uncontrollable aversive object becomes much more salient upon dNPF activation. This highlights the importance of accounting for behavioral control in any understanding of brain functions underlying perception, including flies in open- vs. closed-loop experiments (52).

Beta-like oscillations have been observed previously in the insect brain. For example, recordings in the locust have identified 20- to 30-Hz oscillations associated with processing of olfactory stimuli (77, 78), and comparable oscillations have also been associated with visual attention in flies (40, 79). Additionally, there is increasing evidence that insect brains employ a variety of oscillations, comparable in range with the mammalian brain. These include 7 to 12 Hz (alpha) (80, 81), 20 to 50 Hz (beta and gamma) (80, 82), and even 1 Hz (delta) (83). These oscillations have been shown to be involved in processes such as olfaction, vision, and sleep, suggesting conserved functions that might transcend the differences in brain architecture between insects and mammals. Whether any of these oscillations are functionally comparable remains to be seen. Nevertheless, our current findings suggest that beta-like oscillations might be employed by the insect brain to bind different stimulus features into unified percepts that guide the animal's attention. Although we did not investigate nonvisual stimulus modalities in this study, previous work has demonstrated that odors modulate the amplitude of visually evoked 20- to 30-Hz activity (40), suggesting these oscillations might govern cross-modal binding as well. Whether endogenous 20- to 30-Hz activity in the fly brain is performing a similar function to beta oscillations in the human brain remains an open question. It is, however, possible that oscillatory processes are supported by different brain architectures that have conserved circuit timing relationships through evolution (84–86). Such conservation might be expected if these oscillations were performing a key function for a variety of adaptive behaviors, such as navigation, finding food, or avoiding predators (87, 88). Our study suggests that oscillations in the beta range (20 to 30 Hz) are indeed performing an important phase-locking function to choreograph meaningful information and thereby, guide selective attention. Although mammalian and fly brains are obviously different, they share some organizational principles (28, 89) that could support the preservation of such oscillatory functions (84).

To determine whether the significant phase–amplitude correlations we observed were due to a physiologically relevant shift between SSVEP phases and endogenous 20- to 30-Hz oscillations, rather than just due to increases in stimulation frequency amplitudes, we performed a simulation where we artificially increased the amplitudes of only the SSVEPs while keeping other frequencies constant. In the simulation, we found no effect of LFP amplitudes on ESC (*SI Appendix*, Fig. S12; see *SI Appendix*, *Supplementary Methods*). We then repeated the simulation with a specific increase in 20- to 30-Hz and 30- to 40-Hz amplitudes and also saw no correlation to the SSVEPs. This indicates that the phase correlations observed in real fly brain activity are functionally relevant and not a by-product of multiple superimposed oscillations of varying amplitudes.

Although 20- to 30-Hz activity stood out as relevant for phase locking to attended objects, other endogenous frequencies showed significant changes upon visual stimulation. In open-loop conditions, visual stimulation alone (without NPF activation) led to an increase in phase–amplitude coupling between SSVEPs and endogenous frequencies in the gamma range (30 to 50 Hz). In the mammalian brain, gamma oscillations have been proposed to provide different functions in sensory processing, depending on the frequency range and timing poststimulus induction. For

example, EEG activity in the lower gamma range (30 to 40 Hz) can be elicited by brief and steady visual stimuli, and an increase in oscillatory power for this frequency range can be observed up to 100 ms after stimulation (90). One idea is that these stimulus-locked gamma oscillations might be relevant for rapid (i.e., unconscious) integration processes that might not necessarily be stimulus relevant (91). Nevertheless, gamma oscillations in humans can also be significantly modulated by attention and stimulus saliency (22, 92, 93). In contrast, a nonstimulus-locked component in the gamma range, occurring around 250 to 350 ms after stimulus presentation, has been proposed to be more relevant for object representation (65). Intriguingly, we see a similar frequency shift in the fly brain. In our study, we observed an increase of 30- to 50-Hz phase locking when visual stimuli were presented, while 20- to 30-Hz phase locking predominated upon NPF circuit activation (Fig. 6*B*). In humans, it has been shown that synchronized oscillations in the gamma and beta ranges have a high degree of interdependence, showing a so-called "gamma-to-beta" transition in response to novel auditory stimuli, for example (24). Whether a gamma-to-beta transition is also occurring in the insect brain, associated with visual perception, remains difficult to address because any evidence for perception in flies must ultimately depend on behavior, which occurs on a slower timescale than stimulus-evoked neural oscillations.

By grounding our study on innate visual preferences, we could, however, infer what the flies were most likely paying attention to. We found that an innately attractive visual object evokes a greater response in the fly brain than an aversive object and that this effect is preserved even under open-loop conditions, when flies are not in control. This suggests a neural correlate of object-based attention or in other words, a brain signal that correctly identifies what a fly is paying attention to—even in the absence of correlated behavior. Although this remains speculative, future experiments tapping directly from this brain signal in closed-loop paradigms should be able to test if it indeed provides a level of cognitive control.

Materials and Methods

Experimental Model and Subject Details.

Experimental animals. *D. melanogaster* were reared and maintained using standardized fly media, under a 12-h light and dark cycle at 24 °C. For all experiments, 3- to 10-d-old adult female flies were used. We used dNPF-Gal4 (provided by Ulrike Heberlein, Janelia Research Campus, Ashburn, Virginia) lines crossed to UAS-CsChrimson(x)::mVenus(attp40) (provided by Vivek Jayaraman, Janelia Research Campus, Ashburn, Virginia) for all experiments. Optogenetic activation of CsChrimson was achieved by feeding flies 0.2 mM ATR-supplemented food (Sigma-Aldrich) for 2 d prior to experiments, and animals were maintained in darkness until testing (61). Non–ATR-fed flies (ATR−) were used as genetically identical controls throughout. For experiments in *SI Appendix*, Fig. S3, we used adult female (3 to 10 d past eclosion) Canton S wild-type flies.

Electrophysiology. After preparation (*SI Appendix, Supplementary Methods*), animals were placed on an air-supported ball within a light emitting diode (LED) arena as previously described for behavioral experiments (33). LFP recordings were performed with a micropipette glass electrode (9 to 12 MΩ), preamplified via a field effect transistor (NB Labs), amplified (×10,000), filtered (low: 0.1 Hz, high: 5 kHz; A-M Systems Differential AC Amplifier Model 1700), digitized (Axon Digidata 1440A Digitizer), and sampled at 25 kHz using the data acquisition software AxoGraph X 1.6.9 (Axon Instruments). Before each experiment, the micropipette was dipped into red fluorescent dye (FluoSpheres Carboxylate-Modified Microspheres; 0.5 μm, red fluorescent [580/605], 2% solids) to aid visualization of the electrode position after each experiment (*SI Appendix*, Fig. S1*D*). In order to visualize the dNPF circuit and the recording site, a fixed-stage fluorescence microscope (Olympus S2X16, Olympus) was used before and after the experiment.

Electrode placement within the CX was guided by mVenus labeling of the FB in dNPF-Gal4 flies. A six-axis micromanipulator (Edmund Optics) was used to bring the dye-labeled electrode tip into close proximity of the FB. A former study comparing LFPs across the *Drosophila* brain showed that neural activity in the CX is separable and distinct from surrounding brain areas, such as the optic lobes and antennal lobes (94). Nevertheless, possible influences from surrounding neuropils cannot be entirely excluded due to the small size of the fly brain and distributed electrical properties of LFPs. After placement of the electrode, fly brain activity was checked for visually responsiveness by observing deflections in the LFP due to a brief light flash. If correlated deflections were observed, the experiment was allowed to proceed; otherwise, either the electrode was readjusted, or a new fly was attempted. LFP data were converted from axograph files (.axgn) to Matlab files (.mat) for further analysis.

Experimental setup. The virtual reality arena was set up as described in previous publications (33, 50). The hexagon-shaped arena consisted of six 32 × 32-pixel LED panels (Shenzhen Sinorad Medical Electronics Inc.) (Fig. 1*A*). In its center, a patterned, air-supported Styrofoam ball (40 mg, 15-mm diameter; Spotlight Ltd. Pty.) was used as a walking medium for the tethered flies (Fig. 1*A*). A six-axis micromanipulator (Edmund Optics) was used to position the fly on the ball. Tracking of the fly and ball movements was realized by a camera (Point Grey Laboratories) mounted at the front of the arena, filming at 60 frames per second (fps). The filmed material was analyzed online by FicTrac (51), a custom-made tracking software, operated by Ubuntu Linux (12.10) running on Windows 7 (SP1). To create a situation where the fly controls the position of the stimulus (closed loop), the position of the stimulus on the LED panels was linked to the movements of the ball. This was achieved by linking the output (movement of the ball) of FicTrac with custom-written Python (2.5) scripts (modified after ref. 50), which in turn, generated the visual output with the corresponding stimulus position through VisionEgg software (95). To achieve this, FicTrac extracted the lateral movement (X), the forward movement (Y), and the rotation of the ball (turning angle $\Delta\Theta$) and calculated a fictive path of the fly movements, which was used to generate in a 1:1 translation between the movement of the ball and the rotation on the stimulus within the 360° arena (25-ms delay).

For the optogenetic control of the dNPF circuit, three orange–red LED lights (Luxeon Rebel; 617 nm, 700 mA, LXM2-PH01-00700) were mounted around the arena, focused on the center of the arena. The activation and inactivation of the red LED lights were linked to the position of the visual stimulus in the arena, which was determined by FicTrac and controlled by BlinkStick (Agile Innovative Ltd.), an LED controller board, driven by a custom-written Python (2.7) script. Chrimson was activated with a red light intensity of ∼6 mW/mm^2. *SI Appendix, Supplementary Methods* has analysis.

Behavioral fixation (closed loop). After preparation (*SI Appendix, Supplementary Methods*), the flies were positioned on the air-supported ball in the LED arena (Fig. 1*A*) and allowed to habituate to the new environment and walking situation for about 2 to 3 min. Every fly was tested for at least 5 to a maximum of 10 trials. Flies were presented with two visual stimuli, separated by 180° at any time during a 2-min trial. If a fly was fixating on the bar, it kept the stimulus within its FVF, which we defined as the width of the frontal panel (32 px [60°]) (Fig. 1*A*). In order to determine the efficacy of fixation, we introduced random perturbations, where the bar was displaced every 15 to 30 s by 60° (32px) to the left or to the right (Fig. 1*C*). A successful repositioning had to occur within 10 s in order to be considered as successful fixation after a perturbation. For the analysis of endogenous fly brain activity during perturbations, trials with more than 10-s return time were excluded.

Visual Stimulation for Electrophysiology.

Closed loop. Flies were presented with two different bar sizes, large (8 × 32 px) and small (8 × 14 px), that could be displayed at two different contrasts, low (Red = 0, Green = 140, Blue = 0) and high (Red = 0, Green = 255, Blue = 0), and flicker at two different frequencies, 5.9 and 6.6 Hz, resulting in a combination of 12 conditions for the binary choice experiment (Fig. 1*B*: for simplicity, six conditions are shown; the experiment included additionally the same six conditions but with swapped frequencies). The stimuli were bright objects on dark background, contrary to what we have used in a previous behavioral study (33). We chose this visual context to be consistent with previous frequency-tagging experiments that employed bright stimuli on dark background (52) and to minimize light interference from the arena for our optogenetic activation experiments. The luminosity in the center of the arena where the fly was positioned (15-cm distance from the LED panel) was 110 lx for the dark large bar, 579 lx for the bright large bar, 67 lx for the dark small bar, and 301 lx for the bright small bar. Luminosity was measured with an LX1010BS portable Lux Meter, measured for each stimulus alone at 15-cm distance 10 times, and then averaged. The flicker frequencies consisted of symmetrical on/off square signals (on = off = 1/5.9/2 s and on = off = 1/6.6/2 s). Every fly was tested for at least six conditions per trial. The appearance of a condition depended on the choice behavior of the fly. If it kept a stimulus in its FVF for a walking distance of 5 cm approximately, it was considered as choice, and the next set of stimuli was presented. If the fly

did not make a choice, the set of stimuli was automatically changed after 30 s. The virtual setup for this paradigm was derived from our previous studies (33, 50). A custom-written Python 2.7 script driving a Blinkstick (Agile Innovative Ltd.) activated the red LEDs that were mounted around the arena. Each time the small (26.25°) bar was in the FVF (between 330° and 30°, with 0° being right in the middle of the visual field of the fly), the dNPF pathway was activated by red light (Fig. 3). For synchronization purposes between our LFP recordings and behavior, we installed a single red LED in the lower back of the arena that was programmed to turn on at the start of a trial. This LED was recorded via a photodiode that was connected to the amplifier. The LED activity recorded by the photodiode was digitized and recorded in Axograph in order to synchronize LFP recordings with behavioral data, recorded by FicTrac.

Open Loop.

Open-loop electrophysiology. Flies were presented with two competing visual stimuli (large 60° bar and small 26.25° bar, 41.25° apart) that were both placed in the FVF. We used four different conditions for this paradigm, where we changed the position of each stimulus (left and right) as well as the flicker frequency of the stimuli (5.9 and 6.6 Hz). In order to control for differences in object luminosity, we introduced variability in the contrast of each stimulus by choosing the previous two contrast/luminosity values and randomly assigning one of these values for every cycle of the stimulation, resulting in ∼50% of the stimulation period being high contrast (Red = 0, Green = 255, Blue = 0) and ∼50% of the stimulation period being low (Red = 0, Green = 140, Blue = 0) contrast for each stimulus. The paradigm consisted of a 10-s baseline where no visual stimulus was present (dark arena) followed by a 20-s visual stimulation period and a 10-s baseline in the dark again. For optogenetic stimulation of the dNPF circuit, we activated the red LEDs during the entire 40-s trial for each of the four conditions. This led to eight conditions (four without red light activation and four with red light activation). Each condition was presented at least three times for every fly. The presentation of the conditions was randomized.

Open-loop behavior. Flies were presented with two competing visual stimuli (large 60° bar and small 26.25° bar, 41.25° apart [configuration 1] and 105° apart [configuration 2]). We used 14 different conditions for each configuration, with the competing stimuli differing in position (left vs. right), brightness (bright vs. dark, same values as for all other experiment), size (small vs. large), and flicker frequency (5.9 vs. 6.6 Hz). Each animal was tested for all conditions for both configurations, resulting in 28 randomized trials. Each trial was 2-min long. Flicker frequencies were swapped midtrial (after 1 min) to ensure that all stimuli were presented with both frequencies. For every animal, half of the trials were illuminated with three red LEDs surrounding the arena as already described for the closed-loop experiments. Animal movement was tracked as described for the closed-loop experiments, with the exception that the ball movements were not translated into movements of the stimulus; the visual stimuli remained static. In order to analyze fly walking behavior, we extracted *x*- and *y*-position data for the ball movement (left and right rotation and forward movement, respectively) and calculated the ball rotation. To assign a left or right rotation of the ball, which translated into right or left directed movements of the animal, we binned our data in 3-s bins, resulting in an average of 120 data points (data were recorded at 60 fps); assigned every increasing value a one and decreasing value a zero; and calculated an average. A situation where the fly moves the ball in equal amounts to the left or to the right would thus result in an average rotation value of 0.5 [e.g., (1 + 1 + 0 + 0)/4 = 0.5]. We subtracted 0.5 for the rotation values obtained, resulting in negative (walking to the left) vs. positive values (walking to the right).

Quantification and statistics. FicTrac datasets containing information about fixation behavior were imported for offline analysis in MATLAB 2019 as well as in GraphPad Prism 8.3.0. In order to analyze fixation, the bar positions were converted into polar coordinates, and their mean vector length was calculated using the Circular Statistics Toolbox for MATLAB (96). Furthermore, the distribution of the bar positions and the mean-vector length were tested for nonuniformity using a Rayleigh test for uniformity of circular data using a bin size of 3.34°. Unless stated otherwise, we averaged all trials first per animal and then applied all further statistics for grouped data. Using GraphPad Prism 8.3.0, we first tested all data for normal (Gaussian) distribution using the D'Agostino and Pearson omnibus normality test with a significance level $\alpha = 0.05$. If the data were normally distributed, a *t* test or pairwise *t* test for comparisons was used if appropriate, and an ordinary ANOVA (or repeated measures ANOVA) was used for comparisons of groups. We used a Brown–Forsythe and Welch test to test for significant differences in SDs between the groups and a Benjamini and Hochberg method to test for false discovery rate. A Tukey's multiple comparisons test or Bonferroni correction was used to detect specific differences between groups. If the data were not normally distributed, we used a Wilcoxon rank sum test with a significance level $\alpha = 0.05$ for pairwise comparisons. For group statistics, we used a Kruskal–Wallis test and a Dunn's multiple comparison test to specific differences between groups. Error bar types are stated in the figures. All statistical tests are stated in the figures.

Data Availability. All of the datasets and code supporting the current study are publicly available from the University of Queensland Research Data Management, which is made available via UQ eSpace, the University of Queensland data storage repository https://doi.org/10.14264/43fb51f.

ACKNOWLEDGMENTS. We thank Bruno Rossion and Corentin Jacques for help in data analysis; Matthew Van De Poll for providing visual stimulation code; Karin Nordstrom for helpful discussions; Lucy Heap, Michael Troup, Niki Anthony, and Rowan Tweedale for helpful comments on the manuscript; and Dragan Rangelov for valuable discussions about phase–amplitude coupling analyses. This work was supported by Deutsche Forschungsgemeinschaft Research Fellowship GR 5030/1-1 (to M.J.G.) and by Australian Research Council Discovery Project Grants DP140103184 (to B.v.S.) and DP180100144 (to B.v.S.).

1. M. I. Posner, C. R. Snyder, B. J. Davidson, Attention and the detection of signals. *J. Exp. Psychol.* **109**, 160–174 (1980).
2. W. James, *Principles of Psychology* (Henry Holt and Company, 1890), vol. 2.
3. J. Duncan, Selective attention in the primate visual system. *Can. Psychol.* **35**, 104–105 (1994).
4. D. Sridharan, D. L. Ramamurthy, J. S. Schwarz, E. I. Knudsen, Visuospatial selective attention in chickens. *Proc. Natl. Acad. Sci. U.S.A.* **111**, E2056–E2065 (2014).
5. B. L. de Bivort, B. van Swinderen, Evidence for selective attention in the insect brain. *Curr. Opin. Insect Sci.* **15**, 9–15 (2016).
6. M. A. Fernandes, S. Koji, M. J. Dixon, J. M. Aquino, Changing the focus of attention: The interacting effect of valence and arousal. *Vis. Cogn.* **19**, 1191–1211 (2011).
7. J. Duncan, Selective attention and the organization of visual information. *J. Exp. Psychol.* **113**, 501–517 (1984).
8. E. H. Cohen, F. Tong, Neural mechanisms of object-based attention. *Cereb. Cortex* **25**, 1080–1092 (2015).
9. V. M. Ciaramitaro, J. F. Mitchell, G. R. Stoner, J. H. Reynolds, G. M. Boynton, Object-based attention to one of two superimposed surfaces alters responses in human early visual cortex. *J. Neurophysiol.* **105**, 1258–1265 (2011).
10. K. M. Tye, Neural circuit motifs in valence processing. *Neuron* **100**, 436–452 (2018).
11. L. S. Colzato, N. C. van Wouwe, B. Hommel, Feature binding and affect: Emotional modulation of visuo-motor integration. *Neuropsychologia* **45**, 440–446 (2007).
12. A. F. Rossi, M. A. Paradiso, Feature-specific effects of selective visual attention. *Vision Res.* **35**, 621–634 (1995).
13. A. Revonsuo, J. Newman, Binding and consciousness. *Conscious. Cogn.* **8**, 123–127 (1999).
14. B. H. Pierce, E. A. Kensinger, Effects of emotion on associative recognition: Valence and retention interval matter. *Emotion* **11**, 139–144 (2011).
15. E. Niebur, C. Koch, C. Rosin, An oscillation-based model for the neuronal basis of attention. *Vision Res.* **33**, 2789–2802 (1993).
16. A. K. Engel, W. Singer, Temporal binding and the neural correlates of sensory awareness. *Trends Cogn. Sci.* **5**, 16–25 (2001).
17. B. Treccani, The neuropsychology of feature binding and conscious perception. *Front. Psychol.* **9**, 2606 (2018).
18. B. Moeller, H. Schächinger, C. Frings, Irrelevant stimuli and action control: Analyzing the influence of ignored stimuli via the distractor-response binding paradigm. *J. Vis. Exp.*, 10.3791/51571 (2014).
19. M. A. Schoenfeld *et al.*, Dynamics of feature binding during object-selective attention. *Proc. Natl. Acad. Sci. U.S.A.* **100**, 11806–11811 (2003).
20. S. Ghorashi, K. M. Spencer, Attentional load effects on beta oscillations in healthy and schizophrenic individuals. *Front. Psychiatry* **6**, 149 (2015).
21. W. Klimesch, α-band oscillations, attention, and controlled access to stored information. *Trends Cogn. Sci.* **16**, 606–617 (2012).
22. L. Melloni *et al.*, Synchronization of neural activity across cortical areas correlates with conscious perception. *J. Neurosci.* **27**, 2858–2865 (2007).
23. P. M. Milner, A model for visual shape recognition. *Psychol. Rev.* **81**, 521–535 (1974).
24. C. Haenschel, T. Baldeweg, R. J. Croft, M. Whittington, J. Gruzelier, Gamma and beta frequency oscillations in response to novel auditory stimuli: A comparison of human electroencephalogram (EEG) data with in vitro models. *Proc. Natl. Acad. Sci. U.S.A.* **97**, 7645–7650 (2000).
25. C. Tallon-Baudry, O. Bertrand, C. Delpuech, J. Pernier, Stimulus specificity of phase-locked and non-phase-locked 40 Hz visual responses in human. *J. Neurosci.* **16**, 4240–4249 (1996).
26. J. Ni *et al.*, Gamma-rhythmic gain modulation. *Neuron* **92**, 240–251 (2016).
27. J. B. Isbister *et al.*, A new approach to solving the feature-binding problem in primate vision. *Interface Focus* **8**, 20180021 (2018).
28. A. B. Barron, C. Klein, What insects can tell us about the origins of consciousness. *Proc. Natl. Acad. Sci. U.S.A.* **113**, 4900–4908 (2016).

29. G. A. Horridge, S.-W. Zhang, D. O'Carroll, Insect perception of illusory contours. *Philos. Trans. R. Soc. Lond. B Biol. Sci.* **337**, 59–64 (1992).
30. S. Stach, J. Benard, M. Giurfa, Local-feature assembling in visual pattern recognition and generalization in honeybees. *Nature* **429**, 758–761 (2004).
31. B. Brembs, J. Wiener, Context and occasion setting in *Drosophila* visual learning. *Learn. Mem.* **13**, 618–628 (2006).
32. S. Tang, A. Guo, Choice behavior of *Drosophila* facing contradictory visual cues. *Science* **294**, 1543–1547 (2001).
33. M. J. Grabowska *et al*., Innate visual preferences and behavioral flexibility in *Drosophila*. *J. Exp. Biol.* **221**, jeb185918 (2018).
34. S. Koenig, R. Wolf, M. Heisenberg, Visual attention in flies-dopamine in the mushroom bodies mediates the after-effect of cueing. *PLoS One* **11**, e0161412 (2016).
35. P. Sareen, R. Wolf, M. Heisenberg, Attracting the attention of a fly. *Proc. Natl. Acad. Sci. U.S.A.* **108**, 7230–7235 (2011).
36. B. van Swinderen, Competing visual flicker reveals attention-like rivalry in the fly brain. *Front. Integr. Nuerosci.* **6**, 96 (2012).
37. B. H. Lancer, B. J. E. Evans, J. M. Fabian, D. C. O'Carroll, S. D. Wiederman, A target-detecting visual neuron in the dragonfly locks on to selectively attended targets. *J. Neurosci.* **39**, 8497–8509 (2019).
38. B. van Swinderen, B. Brembs, Attention-like deficit and hyperactivity in a *Drosophila* memory mutant. *J. Neurosci.* **30**, 1003–1014 (2010).
39. B. van Swinderen, Attention-like processes in *Drosophila* require short-term memory genes. *Science* **315**, 1590–1593 (2007).
40. B. van Swinderen, R. J. Greenspan, Salience modulates 20-30 Hz brain activity in *Drosophila*. *Nat. Neurosci.* **6**, 579–586 (2003).
41. B. van Swinderen, "Attention in *Drosophila*" in *Recent Advances in the Use of Drosophila in Neurobiology and Neurodegeneration*, N. Atkinson, Ed. (International Review of Neurobiology, Academic Press, 2011), pp. 51–85.
42. Y. Pan *et al*., Differential roles of the fan-shaped body and the ellipsoid body in *Drosophila* visual pattern memory. *Learn. Mem.* **16**, 289–295 (2009).
43. A. Wystrach, A. D. M. Dewar, P. Graham, Insect vision: Emergence of pattern recognition from coarse encoding. *Curr. Biol.* **24**, R78–R80 (2014).
44. J. D. Seelig, V. Jayaraman, Feature detection and orientation tuning in the *Drosophila* central complex. *Nature* **503**, 262–266 (2013).
45. J. Green, V. Vijayan, P. Mussells Pires, A. Adachi, G. Maimon, A neural heading estimate is compared with an internal goal to guide oriented navigation. *Nat. Neurosci.* **22**, 1460–1468 (2019).
46. J. D. Seelig, V. Jayaraman, Neural dynamics for landmark orientation and angular path integration. *Nature* **521**, 186–191 (2015).
47. K. S. Kakaria, B. L. de Bivort, Ring attractor dynamics emerge from a spiking model of the entire protocerebral bridge. *Front. Behav. Neurosci.* **11**, 8 (2017).
48. S. S. Kim, H. Rouault, S. Druckmann, V. Jayaraman, Ring attractor dynamics in the *Drosophila* central brain. *Science* **356**, 849–853 (2017).
49. G. Maimon, A. D. Straw, M. H. Dickinson, A simple vision-based algorithm for decision making in flying *Drosophila*. *Curr. Biol.* **18**, 464–470 (2008).
50. M. N. Van De Poll, E. L. Zajaczkowski, G. J. Taylor, M. V. Srinivasan, B. van Swinderen, Using an abstract geometry in virtual reality to explore choice behaviour: Visual flicker preferences in honeybees. *J. Exp. Biol.* **218**, 3448–3460 (2015).
51. R. J. D. Moore *et al*., FicTrac: A visual method for tracking spherical motion and generating fictive animal paths. *J. Neurosci. Methods* **225**, 106–119 (2014).
52. A. C. Paulk, L. Kirszenblat, Y. Zhou, B. van Swinderen, Closed-loop behavioral control increases coherence in the fly brain. *J. Neurosci.* **35**, 10304–10315 (2015).
53. D. B. Turner-Evans, V. Jayaraman, The insect central complex. *Curr. Biol.* **26**, R453–R457 (2016).
54. A. M. Norcia, L. G. Appelbaum, J. M. Ales, B. R. Cottereau, B. Rossion, The steady-state visual evoked potential in vision research: A review. *J. Vis.* **15**, 4 (2015).
55. L. Shao *et al*., Dissection of the *Drosophila* neuropeptide F circuit using a high-throughput two-choice assay. *Proc. Natl. Acad. Sci. U.S.A.* **114**, E8091–E8099 (2017).
56. M. J. Krashes *et al*., A neural circuit mechanism integrating motivational state with memory expression in *Drosophila*. *Cell* **139**, 416–427 (2009).
57. S. F. Garczynski, M. R. Brown, P. Shen, T. F. Murray, J. W. Crim, Characterization of a functional neuropeptide F receptor from *Drosophila melanogaster*. *Peptides* **23**, 773–780 (2002).
58. J. P. Redrobe, Y. Dumont, R. Quirion, Y. Neuropeptide, Neuropeptide Y (NPY) and depression: From animal studies to the human condition. *Life Sci.* **71**, 2921–2937 (2002).
59. H. A. Dierick, R. J. Greenspan, Serotonin and neuropeptide F have opposite modulatory effects on fly aggression. *Nat. Genet.* **39**, 678–682 (2007).
60. B. Y. Chung *et al*., *Drosophila* neuropeptide F signaling independently regulates feeding and sleep-wake behavior. *Cell Rep.* **19**, 2441–2450 (2017).
61. N. C. Klapoetke *et al*., Independent optical excitation of distinct neural populations. *Nat. Methods* **11**, 338–346 (2014).
62. A. Keil *et al*., Early modulation of visual perception by emotional arousal: Evidence from steady-state visual evoked brain potentials. *Cogn. Affect. Behav. Neurosci.* **3**, 195–206 (2003).
63. Y. Zhang, Y. Zhang, P. Cai, H. Luo, F. Fang, The causal role of α-oscillations in feature binding. *Proc. Natl. Acad. Sci. U.S.A.* **116**, 17023–17028 (2019).
64. A. HajiHosseini, C. B. Holroyd, Sensitivity of frontal beta oscillations to reward valence but not probability. *Neurosci. Lett.* **602**, 99–103 (2015).
65. C. Tallon-Baudry, O. Bertrand, Oscillatory gamma activity in humans and its role in object representation. *Trends Cogn. Sci.* **3**, 151–162 (1999).
66. R. A. Seymour, G. Rippon, K. Kessler, The detection of phase amplitude coupling during sensory processing. *Front. Neurosci.* **11**, 487 (2017).
67. A. C. E. Onslow, R. Bogacz, M. W. Jones, Quantifying phase-amplitude coupling in neuronal network oscillations. *Prog. Biophys. Mol. Biol.* **105**, 49–57 (2011).
68. M. J. Hülsemann, E. Naumann, B. Rasch, Quantification of phase-amplitude coupling in neuronal oscillations: Comparison of phase-locking value, mean vector length, modulation index, and generalized-linear-modeling-cross-frequency-coupling. *Front. Neurosci.* **13**, 573 (2019).
69. K. von Kriegstein, A.-L. Giraud, Implicit Multisensory Associations Influence Voice Recognition, Implicit multisensory associations influence voice recognition. *PLoS Biol.* **4**, e326 (2006).
70. F. Foroni, G. Pergola, R. I. Rumiati, Food color is in the eye of the beholder: The role of human trichromatic vision in food evaluation. *Sci. Rep.* **6**, 37034 (2016).
71. C. Aissani, J. Martinerie, L. Yahia-Cherif, A.-L. Paradis, J. Lorenceau, Beta, but not gamma, band oscillations index visual form-motion integration. *PLoS One* **9**, e95541 (2014).
72. K. Wimmer, M. Ramon, T. Pasternak, A. Compte, Transitions between multiband oscillatory patterns characterize memory-guided perceptual decisions in prefrontal circuits. *J. Neurosci.* **36**, 489–505 (2016).
73. A. K. Engel, P. Fries, Beta-band oscillations–Signalling the status quo? *Curr. Opin. Neurobiol.* **20**, 156–165 (2010).
74. J. Marco-Pallarés, T. F. Münte, A. Rodríguez-Fornells, The role of high-frequency oscillatory activity in reward processing and learning. *Neurosci. Biobehav. Rev.* **49**, 1–7 (2015).
75. B. Spitzer, S. Haegens, Beyond the status quo: A role for beta oscillations in endogenous content (re)activation. *eNeuro* **4**, ENEURO.0170-17.2017 (2017).
76. E. Perisse *et al*., Aversive learning and appetitive motivation toggle feed-forward inhibition in the *Drosophila* mushroom body. *Neuron* **90**, 1086–1099 (2016).
77. G. Laurent, M. Naraghi, Odorant-induced oscillations in the mushroom bodies of the locust. *J. Neurosci.* **14**, 2993–3004 (1994).
78. J. Perez-Orive *et al*., Oscillations and sparsening of odor representations in the mushroom body. *Science* **297**, 359–365 (2002).
79. S. Tang, M. Juusola, Intrinsic activity in the fly brain gates visual information during behavioral choices. *PLoS One* **5**, e14455 (2010).
80. T. Popov, P. Szyszka, Alpha oscillations govern interhemispheric spike timing coordination in the honey bee brain. *Proc. Biol. Sci.* **287**, 20200115 (2020).
81. M. H. W. Yap *et al*., Oscillatory brain activity in spontaneous and induced sleep stages in flies. *Nat. Commun.* **8**, 1815 (2017).
82. G. Laurent, H. Davidowitz, Encoding of olfactory information with oscillating neural assemblies. *Science* **265**, 1872–1875 (1994).
83. D. Raccuglia *et al*., Network-specific synchronization of electrical slow-wave oscillations regulates sleep drive in *Drosophila*. *Curr. Biol.* **29**, 3611–3621.e3 (2019).
84. G. Buzsáki, N. Logothetis, W. Singer, Scaling brain size, keeping timing: Evolutionary preservation of brain rhythms. *Neuron* **80**, 751–764 (2013).
85. K. Linkenkaer-Hansen, V. V. Nikouline, J. M. Palva, R. J. Ilmoniemi, Long-range temporal correlations and scaling behavior in human brain oscillations. *J. Neurosci.* **21**, 1370–1377 (2001).
86. J. Herberholz, G. D. Marquart, Decision making and behavioral choice during predator avoidance. *Front. Neurosci.* **6**, 125 (2012).
87. H. Haberkern, V. Jayaraman, Studying small brains to understand the building blocks of cognition. *Curr. Opin. Neurobiol.* **37**, 59–65 (2016).
88. L. Chittka, M. Giurfa, J. A. Riffell, Editorial: The mechanisms of insect cognition. *Front. Psychol.* **10**, 2751 (2019).
89. N. J. Strausfeld, F. Hirth, Deep homology of arthropod central complex and vertebrate basal ganglia. *Science* **340**, 157–161 (2013).
90. G. E. Chatrian, R. G. Bickford, A. Uihlein, Depth electrographic study of a fast rhythm evoked from the human calcarine region by steady illumination. *Electroencephalogr. Clin. Neurophysiol.* **12**, 167–176 (1960).
91. I. Fründ, N. A. Busch, J. Schadow, U. Körner, C. S. Herrmann, From perception to action: Phase-locked gamma oscillations correlate with reaction times in a speeded response task. *BMC Neurosci.* **8**, 27 (2007).
92. N. A. Busch, S. Debener, C. Kranczioch, A. K. Engel, C. S. Herrmann, Size matters: Effects of stimulus size, duration and eccentricity on the visual gamma-band response. *Clin. Neurophysiol.* **115**, 1810–1820 (2004).
93. N. A. Busch, J. Schadow, I. Fründ, C. S. Herrmann, Time-frequency analysis of target detection reveals an early interface between bottom-up and top-down processes in the gamma-band. *Neuroimage* **29**, 1106–1116 (2006).
94. A. C. Paulk, Y. Zhou, P. Stratton, L. Liu, B. van Swinderen, Multichannel brain recordings in behaving *Drosophila* reveal oscillatory activity and local coherence in response to sensory stimulation and circuit activation. *J. Neurophysiol.* **110**, 1703–1721 (2013).
95. A. D. Straw, Vision egg: An open-source library for realtime visual stimulus generation. *Front. Neuroinform.* **2**, 4 (2008).
96. P. Berens, CircStat: A MATLAB toolbox for circular statistics. *J. Stat. Softw.* **31**, 1–21 (2009).